nature portfolio

# Peer Review File

## The Growing Charge-Density-Wave Order in CuTe Lightens and Speeds up Electrons

**REVIEWER COMMENTS**

**Reviewer #1 (Remarks to the Author):**

The paper titled "The Charge-Density Wave in CuTe Lightens and Speeds up Electrons" by Wang et al. presents momentum-dependent electron energy-loss spectroscopy experiments on the quasi-1D charge-density wave (CDW) system CuTe. The authors conducted temperature-dependent measurements of energy loss spectra in CuTe, obtaining anisotropic plasmon dispersions. Through the analysis of plasmon behavior using a classic model combined with first-principles calculations, the authors derived the effective mass and Fermi velocity of the Te-px electrons as functions of temperature. Subsequently, they observed a reduction in effective mass and an enhancement in Fermi velocity in the CDW phase, possibly attributable to decreasing correlation and reduced electron density in the CDW phase of the system.

In my view, the experimental investigation of collective excitations in a CDW system is always crucial. This work offers a timely report on the intriguing CDW system CuTe. The authors conducted comprehensive experiments and calculations, presenting in-depth analyses in the manuscript and Supplemental Materials. I believe the results merit publication in some form. However, certain modifications and clarifications are necessary to strengthen the conclusions before considering publication in a prestigious journal like Nature Communications.

1. The primary issue in the paper is the absence of a comparison between the normal phase and the CDW phase. Especially, the effective mass and Fermi velocity in the normal phase were not extracted. For the claim "The Charge-Density Wave in CuTe Lightens and Speeds up Electrons," this comparison is essential and should be emphasized in the figures and text. For example, in Fig. 4, all the data at 335 K and 360 K are missing, which needs attention and inclusion for completeness.

2. Another issue concerns the extraction of the effective mass, which requires information about the screening dielectric constant ε. It appears that the authors used the calculated ε=1.4 for all temperatures, which is a bold assumption and needs further justification. In a CDW system, generally, ε will be strongly temperature-dependent.

3. The descriptions of the linearly-dispersing bands in CuTe are perplexing. If the bands across the Fermi level are strictly linearly dispersing, then the electrons should be massless, implying a zero effective mass. Additionally, the plasmon dispersion equation [Eq.(1) in the manuscript] is typically derived from an electron gas with a parabolic dispersion $E=(\hbar^2 k^2)/2m$. Therefore, applying it to a linearly dispersing electron gas may not be appropriate. If the plasmons discussed in the manuscript arise from parabolic bands, then clarification is needed regarding the descriptions of the linearly-dispersing bands.

There are also some minor issues I suggest the authors to modify:

4. Regarding the statement, “At the Fermi level, the CDW gaps out the Te-px state (Fig. 1d), whereas the Te-py state thereby remains intact (also Fig. 1e),” in Figure 1 (d), no gap in the Te-px band at the Fermi level is visible. Please provide clarification or add visual aids to support this claim.

5. In the colored map in Figure 2 (e) and (f), it appears that the linewidths of the plasmons peculiarly decrease with increasing q. I recommend analyzing the linewidth as a function of q to verify the damping behavior of the plasmons.

6. In Fig. 1b, the arrows indicating the CDW period “5a” do not repeat as expected. Please check this inconsistency.

## POINT-BY-POINT RESPONSES TO THE REVIEWER'S COMMENTS

We have taken into account all opinions of the referee (**BOLD**, for clarity) and our detailed responses are elucidated in the report below. The associated changes made to the manuscript and supplementary information are indicated in RED UNDERLINED for clarity. In addition, we have revised Figs. 1-5, accordingly, and incorporated new supplementary Figs. 1 and 7 that address the respective minor remarks #6 and 5 of the referee. All the other supplementary figures are readily renumbered and supplementary Figs. 4, 8, and 9 are revised, accordingly.

**Reviewer #1 (Remarks to the Author):**

**The paper titled "The Charge-Density Wave in CuTe Lightens and Speeds up Electrons" by Wang *et al.* presents momentum-dependent electron energy-loss spectroscopy experiments on the quasi-1D charge-density wave (CDW) system CuTe. The authors conducted temperature-dependent measurements of energy loss spectra in CuTe, obtaining anisotropic plasmon dispersions. Through the analysis of plasmon behavior using a classic model combined with first-principles calculations, the authors derived the effective mass and Fermi velocity of the Te-$p_x$ electrons as functions of temperature. Subsequently, they observed a reduction in effective mass and an enhancement in Fermi velocity in the CDW phase, possibly attributable to decreasing correlation and reduced electron density in the CDW phase of the system.**

**In my view, the experimental investigation of collective excitations in a CDW system is always crucial. This work offers a timely report on the intriguing CDW system CuTe. The authors conducted comprehensive experiments and calculations, presenting in-depth analyses in the manuscript and Supplemental Materials. I believe the results merit publication in some form. However, certain modifications and clarifications are necessary to strengthen the conclusions before considering publication in a prestigious journal like Nature Communications.**

**Response:**

We appreciate a lot the helpful report of the reviewer and the positive comment on our work. The referee's specific remarks below are thoroughly addressed.

**1. The primary issue in the paper is the absence of a comparison between the normal phase and the CDW phase. Especially, the effective mass and Fermi velocity in the normal phase were not extracted. For the claim "The Charge-**

**Density Wave in CuTe Lightens and Speeds up Electrons," this comparison is essential and should be emphasized in the figures and text. For example, in Fig. 4, all the data at 335 K and 360 K are missing, which needs attention and inclusion for completeness.**

**Response:**

We have taken into account the suggestion of the referee. The light-electron plasmon dispersions in the normal state at 335 ($T_{CDW}$) and 360 K are incorporated into Fig. 4a, and the corresponding effective mass ($m^*$) and carrier density ($n$) appear in Fig. 4b. We show the respective Fermi velocities ($v_F$) at 335 and 360 K in Fig. 5a, which also comprises the revised $v_F$ and graphene-analogy $v_F^G$ below $T_{CDW}$ considering the $m^*$ and $n$ in Fig. 4b that are derived within the framework of a temperature dependence in the screening dielectric constant ($\varepsilon_\infty$, **Remark 2**; supplementary Fig. 4c). In Fig. 4c, the CDW gap and superlattice $q_{CDW}$ vanish above $T_{CDW}$ and, therefore, the figure is not modified. Fig. 4d highlights the systematic blueshift of the light-electron plasmon below $T_{CDW}$ and is revised in accordance with the $v_F$ in Fig. 5a. For the convenience of referee's considerations, supplementary Figs. 4b and 4c, essential for this response session, are exhibited hereinbelow.

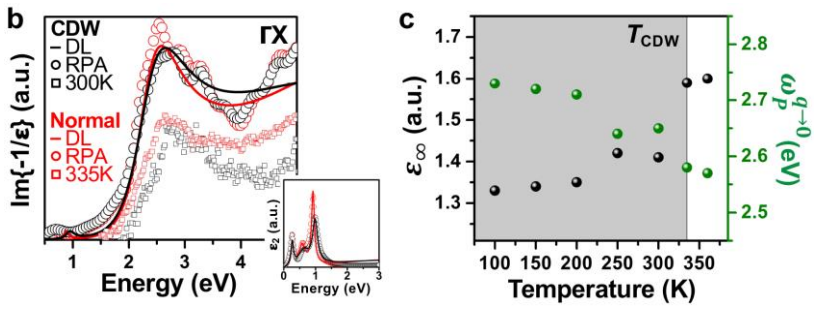


**Supplementary Figure 4 | Experimental and theoretical studies of plasmon dispersions in CuTe. b**, The RPA-theoretical loss functions of the Te-$p_x$ light-electron plasmon along ΓX in respective CDW (black) and normal (red) states at $q$ = 0.1 Å$^{-1}$. Open circles (squares), RPA calculations (EELS at designated temperatures). Inset, the corresponding imaginary parts of the dielectric functions ($\varepsilon_2$; circles, RPA) predominated by three single-particle transitions below the plasmon excitation. Black and red lines, the Drude-Lorentz (DL) modeling of respective RPA dielectric functions (supplementary information B) and the readily derived loss functions. **c**, The temperature-dependent $\varepsilon_\infty$ (black) and associated $\omega_P^{q\to 0}$ (green) used in the $\varepsilon_\infty$ derivations (see also supplementary information B).

Indeed, the light-electron plasmon dispersions above (the normal state; gray inverse triangles, Figs. 3a-d in the main text) and below $T_{CDW}$ (the CDW state; black inverse triangles) are different. Take the CDW-state plasmons at 300 K as the reference (Figs. 3a-d), those in the normal state firstly redshift at $q$ = 0.1 Å$^{-1}$ and then blueshift at $q$ = 0.2-0.4 Å$^{-1}$, dissimilar to the systematic blueshift of the plasmons below $T_{CDW}$. This difference is related to the electronically distinct dielectric functions of the normal and CDW states (inset, supplementary Fig. 4b) and, therefore, $\varepsilon_\infty$ that is essential for the derivation of $m^*$ and $n$ shall also be different in the respective phases. As suggested by the referee in **Remark 2**, $\varepsilon_\infty$ would even be temperature-dependent in the normal or CDW state by itself.

For deriving the temperature-dependent $\varepsilon_\infty$, we conduct Drude-Lorentz modeling of the respective RPA dielectric functions in normal and CDW states (inset, supplementary Fig. 4b), with the Lorentz terms depicting the single-particle absorptive peaks in $\varepsilon_2$ and the Drude term underlining the collective-plasmon oscillation of $\omega_P$. Using the Drude and Lorentz parameters in supplementary Table 1 (also shown below), we achieve the modeling of the RPA dielectric functions (inset, supplementary Fig. 4b). The RPA loss functions and associated EELS at 335 and 300 K are also captured by the DL modeling (supplementary Fig. 4b). The respective Drude-$\omega_P$ components of 3.25 and 3.15 eV in supplementary Table 1 are then exploited for the normal (335 and 360 K) and CDW states (100-300 K) in general, since it is implausible to obtain the RPA dielectric function at each designated temperature.

**Supplementary Table 1 | The physical parameters for the DL modeling of $\varepsilon(\omega)$ in the respective normal and CDW states (all units in eV).**

| Phase | $\omega_P$ | $\gamma_P$ | $\omega_\Delta$ | $\gamma_\Delta$ | $\omega_{T1}$ | $\gamma_{T1}$ | $\omega_{T2}$ | $\gamma_{T2}$ | $\omega_{T3}$ | $\gamma_{T3}$ | $\omega_{T4}$ | $\gamma_{T4}$ |
|---|---|---|---|---|---|---|---|---|---|---|---|---|
| **Normal** | 3.25 | 0.01 | 0 | 0.2 | 0.27 | 0.2 | 0.59 | 0.25 | 0.92 | 0.11 | 4.5 | 5.5 |
| **CDW** | 3.15 | 0.01 | 0.05 | 0.2 | 0.27 | 0.1 | 0.66 | 0.4 | 0.99 | 0.2 | 4.5 | 6.3 |

Based on the notion of $\omega_P^{q\to0} = \frac{\omega_P}{\sqrt{\varepsilon_\infty}}$, we estimate the temperature-dependent $\varepsilon_\infty$, as shown in supplementary Fig. 4c along with the extrapolated $\omega_P^{q\to0}$ at $q$ = 0 Å$^{-1}$ from the EELS results in Fig. 4a (main text). Using these temperature-dependent $\varepsilon_\infty$, we revise $m^*$, $n$, and $v_F$ across $T_{CDW}$ (Figs. 4b and 5a; main text) in accordance with the suggestion of the referee. All figures involve the plasmon-dispersion dependence on

$v_F$ are also revised (Figs. 2e, 2f, 4d in the main text; supplementary Figs. 4d, 4e, 8). In addition, we revise supplementary Fig. 9 using the Drude-Lorentz parameters in supplementary Table 1.

We now tackle the comparison on $m^*$, $n$, and $v_F$ across $T_{CDW}$ (Figs. 4b and 5a; main text). In Fig. 4b, the incorporation of temperature-dependent $\varepsilon_\infty$ (supplementary Fig. 4c) into the derivation of $m^*$ and $n$ remarkably improves the agreement with the inverse BCS scaling. Moreover, the systematic decrease in $n$ across $T_{CDW}$ (Fig. 4b) is closely consistent with the BCS-type CDW gap opening (Fig. 4c). We are aware of a small increase in $m^*$ (0.27 $m_0$, 335 K; 0.28 $m_0$, 300 K; Fig. 4b) and decrease in $v_F$ ($1.68 \times 10^8$ cm s$^{-1}$, 335 K; $1.61 \times 10^8$ cm s$^{-1}$, 300 K; Fig. 5a) across $T_{CDW}$, namely ~4% increase (decrease) in the $m^*$ ($v_F$). Below $T_{CDW}$, the $m^*$, however, significantly decreases by ~21% toward 100 K (0.22 $m_0$) upon the growth of the CDW order (Fig. 4c), and the $v_F$ concomitantly increases by ~19% ($1.91 \times 10^8$ cm s$^{-1}$). The conventional notion on the CDW-correlation effect of enhanced $m^*$ and reduced $v_F$ is only marginal in CuTe and, instead, overwhelmed by the inversely reduced $m^*$ and enhanced $v_F$ upon the growing CDW order toward 100 K (Figs. 4b and 5a). With these $m^*$ and $v_F$ characteristics across $T_{CDW}$, we more explicitly revise the title of our work by "The Growing Charge-Density-Wave Order in CuTe Lightens and Speeds up Electrons" and improve all related contexts throughout the work (changes made in RED UNDERLINED for clarity), accordingly.

**2. Another issue concerns the extraction of the effective mass, which requires information about the screening dielectric constant ε. It appears that the authors used the calculated ε=1.4 for all temperatures, which is a bold assumption and needs further justification. In a CDW system, generally, ε will be strongly temperature-dependent.**

**Response:**

As depicted in the above response to **Remark 1**, we have derived the temperature-dependent $\varepsilon_\infty$ in supplementary Fig. 4c. The readily revised $m^*$ and $n$ (Fig. 4b, main text) show an improved agreement with the inverse BCS scaling. More remarkably, the revised normalized temperature dependences of respective $v_F$ and graphene-analogy $v_F^G$ below $T_{CDW}$ become almost identical (Fig. 5a, main text), insinuating that the primary origin for the reduced $m^*$ and enhanced $v_F$ upon the growing CDW order in CuTe may be alike the effect of reduced electronic screening in the graphene by concomitantly decreased $n$. The suppressed electronic scattering by the frozen CDW

potential in CuTe toward 100 K (Fig. 5d, main text; supplementary information D) may not be the most essential factor for the observed reduced $m^*$ and enhanced $v_F$ below $T_{CDW}$, since the absence of a CDW potential above $T_{CDW}$ does not convey even lighter $m^*$ and faster $v_F$ than those of the electrons at low temperatures. All these aspects are incorporated into the revised manuscript (changes made in RED UNDERLINED for clarity). Indeed, the suggestion of the referee on temperature-dependent $\varepsilon_\infty$ has led to significant improvements in the temperature dependences on $m^*$, $n$, and $v_F$ (Figs. 4b and 5a; main text), which point to the primary role of reduced electronic screening, analogous to that in the graphene, in the reduced $m^*$ and enhanced $v_F$ upon the growing CDW order below $T_{CDW}$. We are grateful for this outstanding remark of the referee.

**3. The descriptions of the linearly-dispersing bands in CuTe are perplexing. If the bands across the Fermi level are strictly linearly dispersing, then the electrons should be massless, implying a zero effective mass. Additionally, the plasmon dispersion equation [Eq.(1) in the manuscript] is typically derived from an electron gas with a parabolic dispersion E=(ħ^2 k^2)/2m. Therefore, applying it to a linearly dispersing electron gas may not be appropriate. If the plasmons discussed in the manuscript arise from parabolic bands, then clarification is needed regarding the descriptions of the linearly-dispersing bands.**

**Response:**

As a generally accepted notion, the symmetry-protected crossing of linearly-dispersing bands is designated for massless fermions harbored at the crossed nodal point (Refs. 1 and 3). The vanishing $m^*$ of this kind in the order of $10^{-2}$ $m_0$ has been reported for the Dirac fermions in graphene (Ref. 2) and topological Dirac semimetal $Cd_3As_2$ [L. P. He *et al*., Phys. Rev. Lett. **113**, 246402 (2014)].

For such massless Dirac fermions in one-, two-, and three-dimensional systems, the corresponding long-wavelength plasmons at $q$ = 0 Å$^{-1}$ turn out to be non-classical and proportional to $1/\sqrt{\hbar}$, while they still obey the same $q$-dispersion dependences as the plasmons in the classical, massive counterparts [S. Das Sarma and E. H. Hwang, Phys. Rev. Lett. **102**, 206412 (2009)]. Only in such massless quantum systems, equation (1) has to be reformulated, accordingly. CuTe is nonetheless topologically trivial by the avoided linear-band crossing (Fig. 1c, main text), lifting the plausibility of a massless character tied to the nodal feature of crossed linearly-dispersing bands. Instead, the practically linearly-dispersing bands of Te-$p_x$ electrons in CuTe (Figs. 1c and 1d; main

text) point to weak electronic correlations of the pertinent carriers with characteristically small $m^*$ (Refs. 4, 13, and 19). Such Te-$p_x$ light electrons with finite $m^*$, as well as the Te-$p_y$ heavy holes that show parabolic band dispersions (Figs. 1c-e, main text), would prompt for the application of equation (1) for pertinent plasmon dispersions. The exploitation of equation (1) for the Te-$p_x$ plasmon gives rise to the asymptotic $m^* \sim 0.22\ m_0$ toward 100 K (Fig. 4b, main text), consistent with $m^* \sim 0.23\ m_0$ by magnetotransport at 2 K (Ref. 23). Equation (1) is apparently compatible with the small, finite $m^*$ of Te-$p_x$ electrons despite their practically linearly-dispersing band features near the Fermi level. In addition, the remarkable agreement between the respective normalized temperature dependences of $v_F$ and graphene-analogy $v_F^G$ below $T_{CDW}$ in Fig. 5a (main text) highlights that the Te-$p_x$ band characteristic near the Fermi level is indeed of the practically linearly-dispersing type with finite $m^*$. Throughout this revised manuscript, we now adopt the description of "practically linearly-dispersing" rather than "linearly-dispersing" for the Te-$p_x$ bands, since the topologically trivial CuTe does not harbor the crossing of linearly-dispersing bands and the former exploitation of "linearly-dispersing" can lead to the ambiguity on massless or massive characters of the pertinent Te-$p_x$ electrons.

All above discussions on the practically linearly-dispersion feature of Te-$p_x$ bands and its compatibility with the classical plasmon-dispersion equation for a free electron gas with given $m^*$ have been incorporated into the revised manuscript (changes made in RED UNDERLINED for clarity). The additional references mentioned above are also considered (now Refs. 39 and 40).

**There are also some minor issues I suggest the authors to modify:**

**4. Regarding the statement, "At the Fermi level, the CDW gaps out the Te-px state (Fig. 1d), whereas the Te-py state thereby remains intact (also Fig. 1e)," in Figure 1 (d), no gap in the Te-px band at the Fermi level is visible. Please provide clarification or add visual aids to support this claim.**

**Response:**

We apologize for this ambiguity in Fig. 1d (main text). Now, we have added a black arrow into the viewgraph to clearly point out the pertinent CDW gap opening near the Fermi level.

**5. In the colored map in Figure 2 (e) and (f), it appears that the linewidths of the**

**plasmons peculiarly decrease with increasing q. I recommend analyzing the linewidth as a function of q to verify the damping behavior of the plasmons.**

**Response:**

The following figure shows the designated plasmon linewidths and clearly reveals the plasmon broadening depicted by the respective Landau damping in Figs. 2e and 2f. The color coding of Figs. 2e and 2f could have rendered the visual effect that the plasmons counterintuitively sharpen at the growth in $q$. To avoid such ambiguities, we have incorporated the following figure into the revised supplementary information as supplementary Fig. 7.

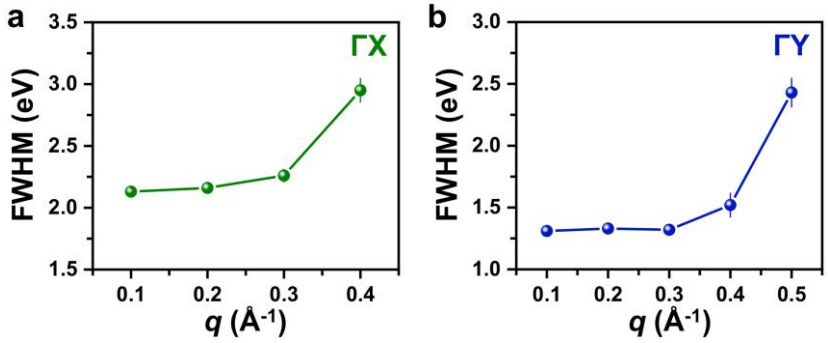


**Supplementary Figure 7 | The full width at half maximum (FWHM) of the plasmons at 300 K along respective ΓX and ΓY. a**, The FWHM of the Te-$p_x$ light-electron plasmons shown in Fig. 2e (300 K; black dots, main text) as a function of $q$. **b**, The FWHM of the Te-$p_y$ heavy-hole plasmons shown in Fig. 2f (300 K; black dots, main text) as a function of $q$. Error bars, standard errors in the associated plasmon-peak fitting.

**6. In Fig. 1b, the arrows indicating the CDW period "5a" do not repeat as expected. Please check this inconsistency.**

**Response:**

To conduct further inspections on Fig. 1b, we remove artworks superimposed on the image, while preserving the arrows and guiding trapezoids (supplementary Fig. 1a). Indeed, there do exist three atomic columns (green circles), where the sign of the atomic displacements within the given trapezoid is inhomogeneously inversed from blue (red) to red (blue). Besides, the arrow sizes across trapezoids do not perfectly follow the $5a \times 2c$ superperiodicity. The two characteristics are associated with effects of noises unavoidably registered in the image by finite sample drifts and mechanical vibrations upon having acquired the series of scanning images. In supplementary Fig. 1b, the image of a sample region close to supplementary Fig. 1a is otherwise immune from the

inhomogeneous arrow-sign problem, but still subject to an imperfect arrow-size repetition with the anticipated superperiodicity of $5a \times 2c$. Our picometer-level evaluations of the atomic displacements [I. C. Lin *et al.*, New J. Phys. **24**, 023011 (2022)] make such effects induced by unavoidable and, meanwhile, very small mechanical noises easily observable (supplementary Figs. 1a and 1b). In supplementary Fig. 1c, the power spectrum of the parent image comprising supplementary Figs. 1a and 1b is shown and it consistently captures the characteristic CDW-superlattice reflections as the electron-diffraction pattern in Fig. 2b (main text), indicating the robust registration of the $5a \times 2c$ superperiodicity in the image despite the unavoidable mechanical noises. All above details on effects of mechanical noises on the imperfect arrow-size repetition with the expected $5a \times 2c$ superperiodicity are incorporated into the revised manuscript (changes made in RED UNDERLINED for clarity), and we replace the CDW-state image in Fig. 1b (main text) by that in supplementary Fig. 1b for a better presentation of the CDW superperiodicity.

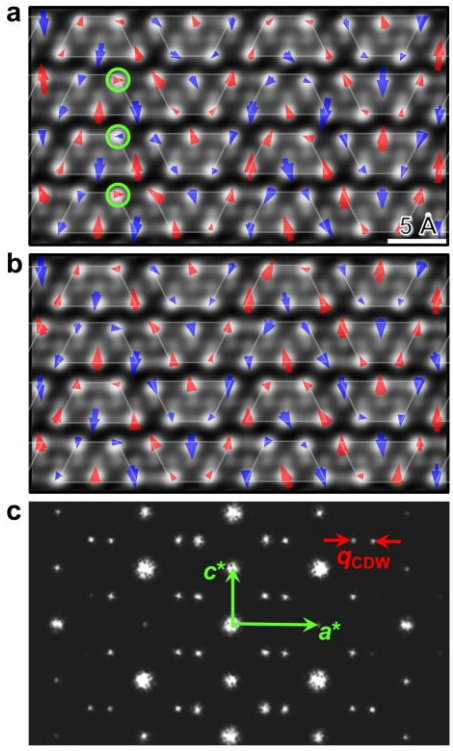


**Supplementary Figure 1 | The STEM imaging and power spectrum of the CDW-state CuTe at 300 K. a**, The CDW-state image corresponding to the original Fig. 1b (main text). **b**, A CDW-state image from a neighboring region to **a**. **c**, The power spectrum of the parent image comprising **a** and **b**, revealing the robust registration of the CDW superperiodicity in the image as those superlattice reflections observed in the electron-diffraction pattern in Fig. 2b (main text).

**REVIEWER COMMENTS**

**Reviewer #1 (Remarks to the Author):**

In the revised version of the manuscript, the authors have thoroughly addressed all of my inquiries and provided extensive modifications. I am impressed with the detailed adjustments made to the experimental results and the analysis, which significantly strengthen the manuscript's conclusions.

Based on these revisions, I am pleased to recommend the acceptance of the manuscript in its current form.

**Reviewer #2 (Remarks to the Author):**

The manuscript describes the investigation of the charge density waves in CuTe using momentum resolved EELS and its interpretation regarding deducing the effective mass and the Fermi velocity of carriers. It is complemented with first-principle calculations. Although the topic is very interesting and novel, more work is needed to produce a more complete manuscript. The experimental approach appears to largely rest on q-EELS which is a difficult, non-standard experimental approach. The validity of the approach needs to be further elaborated on than is currently done to appeal to the readership of Nat Comm. Furthermore, the entire manuscript only references very few (mostly older) prior EELS work even though there is a vast body of recent publications based on EELS (even if slightly adjacent in topics). Prior EELS work on investigating CDW and magnons should be referenced in the introduction and discussed when interpreting results. Aside from this, some of the data is far from convincing in its present form. The manuscript under the present form cannot be published as it contains issues that need to be addressed to make a more convincing case.

1. Literature review regarding q-EELS is missing/incomplete.
2. Specifically, far more details are needed on the q-EELS measurements to explain this to a non-expert reader. This is not yet a standard technique so broad readership will not be familiar with it. It might be useful to add a schematic somewhere to describe this approach and how the information measured is used in the manuscript.
3. Far more actual experimental details are needed in the methodology for reproducibility. Currently, general statements regarding resolution are made but this information does not say much. Resolution limits of the instruments are not the limiting factor in these measurements since energy, momentum and spatial resolutions cannot be maximised simultaneously. This needs to be explained in the methods section. Also add what the actual resolution was that was achieved in the specific measurements. What are the acquisition parameters?
4. What method was used for the q-EELS? It seems that a circular aperture method was used but I could not find this information anywhere.
5. Experimentally, spectra associated with Gamma- X shown in Fig2 c and the map e are far from convincing. For instance – what is happening to the dispersion above 0.2A-1. Comment on the discrepancies compared to theory.
6. EEL spectra should be background removed for the ZLP as the peaks appear to sit on the tail of the ZLP and this would induce a non-consistent shift that might vary with increasing momentum transfer.

7. Fig 3: panel d- it seems that the signal is not above noise. It appears that the fitting shown in SI Fig 6 is just fitting of the shoulder of the higher energy-loss peak.
8. Many of the peak fittings appears highly unreliable. Combined with the absence of ZLP removal make the interpretation of a shift unreliable. In the manuscript l 207: …manifests a systematic blueshift with decreasing temperatures below TCDW… This is therefore an overstatement considering the poor-signal to noise levels of the data and the questionable fitting. The determination of the peak maxima is crucial to determine the slope of the dispersion. And must of the rest of the argumentation appears to relies on this which makes it even more important to get this right. This is a weak point of the manuscript.
9. A-EELS is not a commonly used abbreviation and should be replaced with EELS.
10. The spectra from the core-loss EELS maps shown in Fig 5 should be added to the SI. What do the spectra look like, especially of the high energy edges for Cu? How was the processing done?
11. In the manuscript it is stated that…the intense quasi-elastic tail buries these plasmons that are much weaker than the bulk valence plasmon dispersing from ~17 eV.. why does it bury it when it happens at very different energies? This should remain resolvable at q=0.

## POINT-BY-POINT RESPONSES TO THE REVIEWERS' COMMENTS

We appreciate the suggestion of Reviewer #1 for the acceptance of our work. It is also encouraging that Reviewer #2 found our report interesting and novel. In this letter of point-by-point responses to the reviewers' comments, all remarks of Reviewer #2 are thoroughly addressed. The related changes made throughout the manuscript and supplementary information are in RED for clarity, including new supplementary Figs. 1 and 4 and supplementary information A. Moreover, Figs. 2c, 2d, and 3 in the main text and supplementary Fig. 8 have been updated by the zero-loss-peak removed forms.

### Reviewer #1 (Remarks to the Author):

**In the revised version of the manuscript, the authors have thoroughly addressed all of my inquiries and provided extensive modifications. I am impressed with the detailed adjustments made to the experimental results and the analysis, which significantly strengthen the manuscript's conclusions.**

**Based on these revisions, I am pleased to recommend the acceptance of the manuscript in its current form.**

**Response:**

We are delighted with the strong endorsement of the referee.

### Reviewer #2 (Remarks to the Author):

**The manuscript describes the investigation of the charge density waves in CuTe using momentum resolved EELS and its interpretation regarding deducing the effective mass and the Fermi velocity of carriers. It is complemented with first-principle calculations. Although the topic is very interesting and novel, more work is needed to produce a more complete manuscript. The experimental approach appears to largely rest on q-EELS which is a difficult, non-standard experimental approach. The validity of the approach needs to be further elaborated on than is currently done to appeal to the readership of Nat Comm. Furthermore, the entire manuscript only references very few (mostly older) prior EELS work even though there is a vast body of recent publications based on EELS (even if slightly adjacent in topics). Prior EELS work on investigating CDW and magnons should be referenced in the introduction and discussed when interpreting results. Aside from this, some of the data is far from convincing in its present form. The manuscript under the present form cannot be published as it contains issues that need to be addressed to make a more convincing case.**

**Response:**

We deeply appreciate that the referee found our work interesting and novel. In this resubmission, we have incorporated the scattering physics of *q*-EELS, more references pertinent to charge-density waves (CDWs) and magnons, and details on the experimental conditions and spectra. New supplementary Figs. 1 (also supplementary information A) and 4 have been incorporated in responses to referee's respective **Remarks 2 and 11** below, with renumbering of the other supplementary figures and information sections. Furthermore, Figs. 2c, 2d, and 3 in the main text and supplementary Fig. 8 have been updated by the zero-loss-peak (ZLP) removed forms. All **Remarks 1~11** are thoroughly addressed.

**1. Literature review regarding q-EELS is missing/incomplete.**

**Response:**

We have cited some earlier and recent *q*-EELS reports (Refs. 29, 35, 40, and 43-45), whereas we focused on the absence of attempts to derive $m^*$ and $v_F$ therein instead of the relevance to CDWs. In this revised manuscript, we incorporate references that address the *q*-EELS probing of plasmons in CDW-material systems (new Refs. 28, 30-34; in addition to old Refs. 29 and 35) and the tackling of magnons (new Refs. 52-54). To be specific, Ref. 29 revisits Ref. 28 [Kogar, A. *et al.*, Science **358**, 1314-1317 (2017)] that reports on the softening and condensation of the plasmon in 1*T*-$TiSe_2$ at the characteristic modulation wave vector below the CDW transition temperature ($T_{CDW}$). Ref. 29 unveils that the designated plasmon in Ref. 28 is, in effect, an inherent phonon mode and the plasmon should locate at a slightly higher energy, which is close to the opening CDW-gap size below the $T_{CDW}$ and thus dramatically attenuated by the gapping. In the 2*H* class of the transition-metal-dichalcogenide family (e.g., 2*H*-$NbSe_2$ and 2*H*-$TaSe_2$; Refs. 30 and 31), a likewise negative dispersion of the plasmon has been observed and attributed to the impact of the CDW order below the $T_{CDW}$. The negative plasmon dispersion was nonetheless proven to be irrelevant with the CDW instability and is merely a band-structure effect that depicts the persistence of an interband transition above the plasmon and screening the collective excitation down to a lower energy (leading to the negative dispersion; Refs. 32 and 33). The plasmons in the CDW materials of $(TaSe_4)_2I$ (Ref. 34) and $K_{0.3}MoO_3$ (Ref. 35) had also been studied by *q*-EELS, while the experiments were conducted above the $T_{CDW}$ and did not scrutinize the respective correlations of the plasmons with the CDWs. In comparison, we resolve the firm $q^2$-dispersion of the plasmons in CuTe and establish the effect of the CDW order

on the plasmon dispersion. Besides, the *q*-EELS investigations on the quanta of the collective magnetic excitations of magnons attract growing interests (Refs. 52-54) and require state-of-the-art EELS with meV resolution that is indispensable for probing phonons and magnons typically at few tens of meV (Ref. 54). Indeed, the *q*-EELS probing of magnon dispersions is complementary to the conventional tackling by inelastic neutron scattering with low scattering cross sections and deserves future devotions (Ref. 54). All above essences are incorporated into the revised manuscript and the changes made are in RED for clarity.

**2. Specifically, far more details are needed on the q-EELS measurements to explain this to a non-expert reader. This is not yet a standard technique so broad readership will not be familiar with it. It might be useful to add a schematic somewhere to describe this approach and how the information measured is used in the manuscript.**

**Response:**

A scheme on *q*-EELS is incorporated as new supplementary Fig. 1 (also shown below; Ref. 25) and all the following supplementary figures are renumbered, accordingly.

As indicated in the scheme, a given electronic excitation ($\Delta E$) is subject to the inelastic scattering with the momentum ($q$) and energy ($\Delta E$) transfers to the material. The $q$ is composed by the $q_{\parallel}$ and $q_{\perp}$, and the $q_{\parallel}$ is formulated by $q_{\parallel} = k_0\theta_{\Delta E}$, with the scattering angle $\theta_{\Delta E}$ being of $\theta_{\Delta E} = \frac{\Delta E}{2E_0}$ ($E_0$, the energy of the incident-electron beam; 200 kV hereby) and $k_0$ being the incident electron-beam wave vector. The $\theta_{\Delta E}$ is characteristically very small and much smaller than the elastic Bragg-scattering angle of $2\theta_B$ ($2d \sin\theta_B = \lambda$, where $d$ being the atomic-plane spacing and $\lambda$ the electron wavelength of 0.0251 Å at 200 kV), rendering the $q_{\parallel}$ to be practically parallel to $k_0$. The $q$ for *q*-EELS is, therefore, largely dominated by the $q_{\perp}$ with $q_{\perp} = k_0\theta$ and $q = \sqrt{q_{\perp}^2 + q_{\parallel}^2}$.

The experimental undertaking of *q*-EELS is achieved by collecting the inelastically scattered electrons at the designated $q_{\perp}$ in between two Bragg spots that depict the symmetry line of interest in reciprocal space (Fig. 2a, main text). For warranting an ultimate correctness in the *q*-EELS probing, $q_{\perp}$ is to be larger than the accompanied momentum resolution ($\Delta q$) of the experimental setup and, ubiquitously, $\Delta q \gg q_{\parallel}$. In our experiments, $\Delta q$ is of ~0.09 Å$^{-1}$ upon the exploitation of a circular EELS-

collection aperture of 2.5 mm in diameter and a diffraction-pattern projection length of 6.8 m ($\Delta q \approx \frac{0.0025}{6.8} \times k_0 \approx$ 0.09 Å$^{-1}$). For tackling the light-electron and also heavy-hole plasmons, the $q_\perp$ is readily optimized as 0.1 Å$^{-1}$ and leads to the condition of $q = \sqrt{q_\perp^2 + q_\parallel^2} \approx q_\perp$ with $q_\perp \gg q_\parallel$. In Figs. 2c-2g and 3 in the main text and supplementary Fig. 6a, the spectral acquisitions were achieved by displacing the diffraction pattern along ΓX or ΓY with the $q_\perp$ step of 0.1 Å$^{-1}$ (i.e., $q \approx q_\perp \gg q_\parallel$) and, for simplicity, we denote $q$ instead of $q_\perp$ throughout the work, as the $q$-EELS convention in Ref. 25 and also Refs. 30-35 (therein, $q \approx q_\perp \gg q_\parallel$ as well). We have incorporated all above details into 'Methods' (the $q$-EELS experimental setup) and 'supplementary information A', with the changes made in RED for clarity.

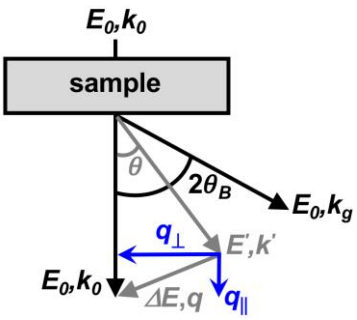


**Supplementary Figure 1 | The inelastic electron scattering upon $q$-EELS.** The inelastic scattering (gray) for plasmon excitations is subject to the respective energy and momentum transfers of $\Delta E$ and $q$, with respect to the incident electron beam (energy, $E_0$; wave vector, $k_0$). The elastic Bragg scattering (wave vector, $k_g$) is also indicated. The $q$ vector consists of the $q_\parallel$ and $q_\perp$, with $q_\parallel = k_0\theta_{\Delta E}$ ($\theta_{\Delta E} = \frac{\Delta E}{2E_0}$). The $\theta_{\Delta E}$ is far smaller than the Bragg scattering angle ($2\theta_B$) and casts the $q_\parallel$ vector being very small. The $q$ for $q$-EELS is, therefore, largely dominated by the $q_\perp$ with $q_\perp = k_0\theta$ and $q = \sqrt{q_\perp^2 + q_\parallel^2}$. The $q_\perp$ is typically larger than the associated experimental momentum resolution $\Delta q$ ($\Delta q \gg q_\parallel$) and leads to the condition of $q = \sqrt{q_\perp^2 + q_\parallel^2} \approx q_\perp$, which forms the scattering basis of the $q$-EELS experimental setup.

**3. Far more actual experimental details are needed in the methodology for reproducibility. Currently, general statements regarding resolution are made but this information does not say much. Resolution limits of the instruments are not**

**the limiting factor in these measurements since energy, momentum and spatial resolutions cannot be maximised simultaneously. This needs to be explained in the methods section. Also add what the actual resolution was that was achieved in the specific measurements. What are the acquisition parameters?**

**Response:**

In the above response to **Remark 2** of the referee, we have elucidated the scattering scheme in our *q*-EELS and the concomitant momentum resolution achieved. The energy resolution of 0.54 eV of our EELS apparatus is robust within 2 seconds of the *q*-EELS spectral acquisitions at $q$ = 0~0.3 Å$^{-1}$. Thanks to the notable stability of our facility and lab environment, the longer acquisitions of 6~8 seconds required for $q \geq$ 0.4 Å$^{-1}$ due to the notably weaker electronic excitations marginally change the energy resolution to 0.57~0.63 eV and such a small change in the energy resolution does not noticeably affect the spectral line-shapes. Moreover, each *q*-EELS spectrum shown in our work is the summation of nine individual spectra with high spectral reproducibility. We had thought that these experimental details could be too subtle for the general readership and, therefore, decided to leave them. We have now incorporated them into 'Methods' (the *q*-EELS experimental setup; RED for clarity).

**4. What method was used for the q-EELS? It seems that a circular aperture method was used but I could not find this information anywhere.**

**Response:**

As elucidated in the response to **Remark 2** of the referee, we have used a circular EELS aperture of 2.5 mm in diameter and this information is now in 'Methods' (the *q*-EELS experimental setup; RED for clarity).

**5. Experimentally, spectra associated with Gamma- X shown in Fig2 c and the map e are far from convincing. For instance – what is happening to the dispersion above 0.2A-1. Comment on the discrepancies compared to theory.**

**Response:**

In the manuscript, we had addressed that the Landau damping would theoretically set in at the crossover of the calculated plasmon dispersion (black line, Fig. 2e; main text) and single-particle continuum (white line, Fig. 2e) at $q$ ~ 0.29 Å$^{-1}$, above which the plasmon should damp into electron-hole pairs and become readily broadened. Experimentally, we do observe the growing damping of the plasmon at $q$ = 0.3 and 0.4 Å$^{-1}$ (Fig. 2c, main text; the corresponding plasmon linewidths, supplementary Fig. 9a).

At $q \geq 0.5$ Å$^{-1}$, the light-electron plasmon becomes heavily damped and indistinguishable (see the rebuttal figure below for the $q$-EELS at $q = 0.5$ Å$^{-1}$). The spectra above $q = 0.5$ Å$^{-1}$ are thus omitted in Fig. 2c for simplicity, while kept in Fig. 2e for the mapping presentation up to the ΓX-zone boundary. A theory-experiment agreement is indeed found in Figs. 2c and 2e. Moreover, the firm quadratic plasmon dispersion in Fig. 2e rules out the arguable negative plasmon dispersion in CDWs (Refs. 30 and 31) and plasmon condensation toward the modulation wave vector (Ref. 28; correspondingly $q_a$, Fig. 2e).

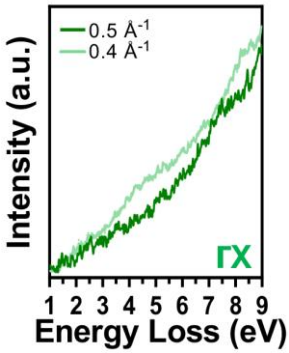


**Rebuttal Figure | The ZLP-removed spectra of the light-electron plasmons at 300 K.** The light-electron plasmons at $q = 0.4$ and 0.5 Å$^{-1}$. For the convenience of comparisons, the intensity of the spectrum at $q = 0.5$ Å$^{-1}$ is normalized to that at 1 eV of the $q = 0.4$ Å$^{-1}$ spectrum.

Nonetheless, Figs. 2c and 2e do exhibit a technical imperfection about the difference in spectral intensities below 1.5 eV, and this difference is related to the previous exploitation of original and ZLP removed spectra in Figs. 2c and 2e, respectively. In Fig. 2c (also Figs. 2d and 3, main text), we had decided to show the original spectra without the removal of ZLP in order to convey an overall view of the experimental spectra for the general readers, who may not have EELS expertise.

For having achieved the dispersion map (Fig. 2e) and the determination of the plasmon-peak positions with an optimal accuracy (results: black dots, Figs. 2e and 2f; data points, Fig. 2h; inverse triangles, Fig. 3; data points, Figs. 4a and 4d; all data points, supplementary Figs. 6d, 6e, 8, 9, and 10), we had nonetheless known that the ZLP removal is imperative. Supplementary Fig. 6b had shown two such ZLP-removed spectra (300 and 335 K) and Fig. 2e (also Figs. 2f and 2g, main text; supplementary Fig. 6a) had been the result derived from the ZLP-removed spectra, though both having not been particularly mentioned. Furthermore, we had used the common ZLP-removal method of fitting the pre-measured ZLP registered in the same experimental conditions

at given $q$'s. Our plasmon-peak position fittings (e.g., results: black dots, Figs. 2e and 2f) had been based on the ZLP-removed spectra as demonstrated in the updated supplementary Fig. 8. The previous form of supplementary Fig. 8 had shown the original spectra for the same sake of a global spectral view for the general readers.

In this revised manuscript, all spectra shown in Figs. 2c, 2d, and 3 (main text) and supplementary Fig. 8 are now in the ZLP-removed forms and the related changes made in the manuscript are in RED for clarity. The inconsistent spectral intensities below 1.5 eV in the previous form of Figs. 2c and 2e due to the respective exploitations of original and ZLP-removed spectra no longer exist.

**6. EEL spectra should be background removed for the ZLP as the peaks appear to sit on the tail of the ZLP and this would induce a non-consistent shift that might vary with increasing momentum transfer.**

**Response:**

As addressed in the above response to **Remark 5** of the referee, all results associated with plasmon-dispersion maps and plasmon-peak positions in the work had been based on ZLP-removed spectra, though having not been particularly mentioned. In this revised manuscript, we have consistently shown the ZLP-removed spectra in pertinent Figs. 2c, 2d, and 3 (main text) and supplementary Fig. 8. The related changes in the manuscript are in RED for clarity.

**7. Fig 3: panel d- it seems that the signal is not above noise. It appears that the fitting shown in SI Fig 6 is just fitting of the shoulder of the higher energy-loss peak.**

**Response:**

Due to the incorporation of new supplementary Figs. 1 and 4, supplementary Fig. 6 has now been renumbered as supplementary Fig. 8. In the revised Fig. 3d (main text) and associated supplementary Fig. 8c, the designated spectra $q$ = 0.4 Å$^{-1}$ are now in the ZLP-removed forms. As theoretically denoted in the above response to **Remark 5**, the plasmon has largely decayed into electron-hole pairs at $q$ = 0.4 Å$^{-1}$ and becomes a damped collective excitation by itself. Therefore, the plasmon at $q$ = 0.4 Å$^{-1}$ has to be weak and broad as what one observes in Fig. 3d, while still well discernible from the spectral background so as to enable our plasmon-peak fittings in supplementary Fig. 8c. The readily fitted plasmon-peak positions at $q$ = 0.4 Å$^{-1}$ are consistent with the theoretical predictions at 300 K (black curve, Fig. 2e; main text) and also those at 250,

200, 150, and 100 K (red curves, Fig. 4d; main text) despite the weak and broad plasmon feature at this large $q$. These further details have been incorporated into the revised manuscript (RED for clarity).

**8. Many of the peak fittings appears highly unreliable. Combined with the absence of ZLP removal make the interpretation of a shift unreliable. In the manuscript l 207: …manifests a systematic blueshift with decreasing temperatures below TCDW… This is therefore an overstatement considering the poor-signal to noise levels of the data and the questionable fitting. The determination of the peak maxima is crucial to determine the slope of the dispersion. And must of the rest of the argumentation appears to relies on this which makes it even more important to get this right. This is a weak point of the manuscript.**

**Response:**

As indicated in the above responses to **Remarks 5-7**, our plasmon-peak fittings at all $q$'s had been achieved on the basis of ZLP-removed spectra, though having not been particularly mentioned, and all pertinent figures (Figs. 2c, 2d, and 3, main text; supplementary Fig. 8) have now been in the ZLP-removed forms. The related experimental argument on a plasmon blueshift below $T_{CDW}$ is corroborated by the theoretical unveiling of the plasmon blueshift below $T_{CDW}$ (Fig. 4d) due to reduced $m^*$ and enhanced $v_F$, providing the reliability in our plasmon-peak fittings with a fundamental evidence.

In revised supplementary Fig. 9 (also shown below), we further incorporate the fitted peak-intensity maxima (normalized to those of the simultaneously acquired bulk plasmons) and show that the plasmon weakening and broadening are conjugated phenomena, as depicted in the physics of plasmon dispersions (Ref. 25). The consistency in the concomitant plasmon broadening and weakening (supplementary Fig. 9) further strengthens the reliability of our plasmon-dispersion slope determinations. The essence of these details is incorporated into the revised manuscript (RED for clarity).

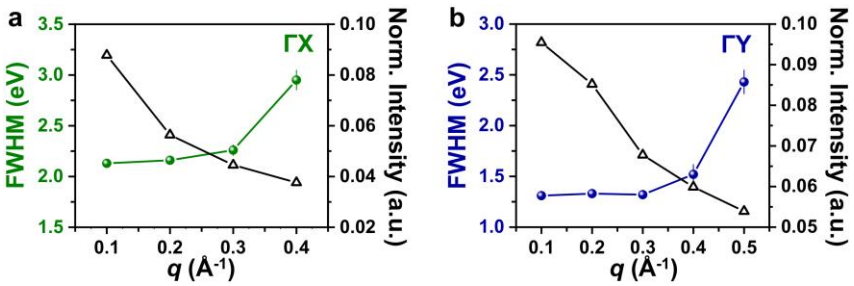


**Supplementary Figure 9 | The full width at half maximum (FWHM) and fitted peak-intensity maxima of the plasmons at 300 K along respective ΓX and ΓY. a**, The fitted FWHM linewidths (green) of the Te-$p_x$ light-electron plasmons shown in Fig. 2e (300K; black dots, main text) as a function of $q$ and derived from the plasmon-peak fittings in supplementary Fig. 8. The simultaneously derived plasmon-peak intensity maxima (black), normalized to those of the respective bulk plasmons acquired in the same time. **b**, The fitted FWHM linewidths (blue) and normalized peak-intensity maxima (black) of the Te-$p_y$ heavy-hole plasmons shown in Fig. 2f (300 K; black dots, main text) as a function of $q$. Error bars, standard errors in the associated plasmon-peak fittings and those for the peak-intensity maxima omitted for simplicity. The observed plasmon broadening in **a** and **b** is consistent with the respective Landau damping depicted in Figs. 2e and 2f (main text). The concomitant plasmon weakening is also consistent with the classical physics for damped collective plasmon excitations.

**9. A-EELS is not a commonly used abbreviation and should be replaced with EELS.**

**Response:**

We have replaced Å-EELS with STEM-EELS in light of the characterization in the STEM mode. The corresponding changes made in the revised manuscript are in RED for clarity.

**10. The spectra from the core-loss EELS maps shown in Fig 5 should be added to the SI. What do the spectra look like, especially of the high energy edges for Cu? How was the processing done?**

**Response:**

The core-level STEM-EELS spectra corresponding to Figs. 5b and 5c had already been shown in supplementary Fig. 12, with the incorporation of the reference spectra from Cu- and Te-metal foils ($Cu^0$ and $Te^0$ in the respective nominal valence states). The STEM-EELS datasets on the CuTe and reference-metal foils had been firstly subject to the random-noise reduction by the principal-component analysis and then the power-

law background removal prior to the respective Cu-*L* and Te-*M* edge retrievals (Refs. 48-50). The spectra of the Te-1 and Cu-1 atoms shown in supplementary Fig. 12 are the respective integrals of 2 × 2 pixels underneath (pixel size, ~0.4 Å) and those of all Te and Cu atoms are the integrals of all the associated atoms in the 5*a* × 2*c* supercell of the CDW. The STEM-EELS elemental mapping of Te and Cu was accomplished by integrating the respective spectral intensities centered at the indicated vertical lines in supplementary Fig. 12 (bottom panels) with the integral-window size of 2 eV. The reference Cu- and Te-foil spectra are the integrals over 30 × 30 pixels, respectively. All these details are now incorporated into 'Methods' (the STEM-EELS experiments; RED for clarity).

**11. In the manuscript it is stated that…the intense quasi-elastic tail buries these plasmons that are much weaker than the bulk valence plasmon dispersing from ~17 eV.. why does it bury it when it happens at very different energies? This should remain resolvable at q=0.**

**Response:**

In the figure below (now, new supplementary Fig. 4), we show the respective ΓX light-electron and ΓY heavy-hole plasmons at 300 K at $q$ = 0 and 0.1 Å$^{-1}$, with spectral-intensity normalizations to the bulk-plasmon intensities at ~17 eV.

At $q$ = 0 Å$^{-1}$, the dynamical nature of electron scattering and finite momentum resolution of our setup cooperatively lead to appreciable spectral intensities below 3 eV and this conventionally termed quasi-elastic tail (Refs. 35 and 40; also Ref. 41: Reimer, L. *Transmission Electron Microscopy*, Chapter 7, Theory of Electron Diffraction; 4$^{th}$ edition, Springer Berlin, 1997) masks the light-electron and heavy-hole plasmons that are essentially an order of magnitude weaker than the bulk plasmons (supplementary Figs. 5c, 5d, and 9). By breaking the dynamical-scattering condition that is most prominent at $q$ = 0 Å$^{-1}$ through the off-$q$ setup (such as $q$ = 0.1 Å$^{-1}$ hereby; meanwhile, having preserved the same momentum resolution), the intense tails can be significantly diminished and the light-electron and heavy-hole plasmons become resolvable. The persistent ZLP at $q$ = 0.1 Å$^{-1}$ and also larger $q$'s is assisted by the electron-phonon scattering, which prevails throughout the entire Brillouin zone (Refs. 25 and 41). We have incorporated these details into the revised manuscript (RED for clarity).

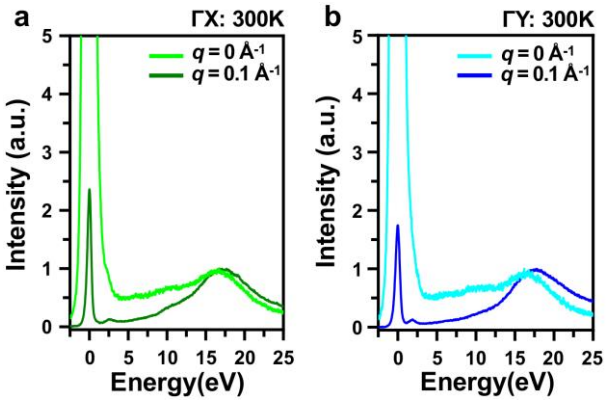


**Supplementary Figure 4 | The ΓX light-electron and ΓY heavy-hole plasmons at $q$ = 0 and 0.1 Å$^{-1}$ at 300 K.** The intense tails at $q$ = 0 Å$^{-1}$ in **a** and **b** due to the dynamical nature of electron scattering mask the plasmon excitations that are essentially an order of magnitude weaker than the bulk plasmons (supplementary Figs. 5c, 5d, and 9). By breaking the dynamical-scattering condition that is most prominent at $q$ = 0 Å$^{-1}$ through the off-$q$ setup (such as $q$ = 0.1 Å$^{-1}$ hereby; meanwhile, having preserved the same momentum resolution), the intense tails can be significantly diminished and the light-electron and heavy-hole plasmons become resolvable. The persistent ZLP at $q$ = 0.1 Å$^{-1}$ and also larger $q$'s is assisted by the electron-phonon scattering, which prevails throughout the entire Brillouin zone.

**REVIEWER COMMENTS**

Reviewer #3 (Remarks to the Author):

The updated manuscript is certainly much improved. The authors have now included a lot of the basic theory underlying the scattering geometry. More importantly, the missing information regarding the actual acquisition parameters have been added into the methodology section. This is of importance to ensure reproducibility.

There are still some questions that remain regarding the data processing. While looking at SI figure 4 for instance one can see that there is significant changes in the ZLP width when increasing q. There is also significant overlap with the signal. This makes a simple background fitting removal using a power law highly unreliable. It is of great importance here to achieve an accurate ZLP removal since the peak positions might shift depending on the quality of the fit. A Richardson-Lucy deconvolution is a standard approach that is widely used to achieve this. What is the reason for using a window fitting method instead?

## POINT-BY-POINT RESPONSES TO THE REVIEWER'S COMMENTS

In this letter of point-by-point responses to the Reviewer's comments, we have addressed all remarks of the Referee and revised supplementary Fig. 4, accordingly, with new insets in supplementary Figs. 4a-b and new supplementary Figs. 4c-f. The associated changes made in Methods in the main text and also supplementary information are in RED for clarity.

### Reviewer (Remarks to the Author):

**The updated manuscript is certainly much improved. The authors have now included a lot of the basic theory underlying the scattering geometry. More importantly, the missing information regarding the actual acquisition parameters have been added into the methodology section. This is of importance to ensure reproducibility.**

**There are still some questions that remain regarding the data processing. While looking at SI figure 4 for instance one can see that there is significant changes in the ZLP width when increasing q. There is also significant overlap with the signal. This makes a simple background fitting removal using a power law highly unreliable. It is of great importance here to achieve an accurate ZLP removal since the peak positions might shift depending on the quality of the fit. A Richardson-Lucy deconvolution is a standard approach that is widely used to achieve this. What is the reason for using a window fitting method instead?**

### Response:

It is encouraging that the referee found our revised manuscript much improved.

Regarding Referee's comments on the ZLP removal, we would like to point out that the power-law background removal mentioned by the Reviewer is a standard method for processing core-level spectra [A. Gloter *et al.*, *Ultramicroscopy* **96**, 385-400 (2003)] and we had faithfully used it for the STEM-EELS core-level characterizations in Figs. 5b-c (main text) and supplementary Fig. 12. In addition, the exploitation of a spectral window (2 eV) for spectral-intensity integrations had been to achieve the STEM-EELS core-level mapping (Fig. 5b, main text). These experimental details had been elucidated in "The STEM-EELS experiments" in Methods (main text). Neither the power-law background removal nor a window fitting method had been conducted for the *q*-EELS spectra of plasmon excitations.

To remove the ZLP in all *q*-EELS spectra, we had undertaken the common ZLP-removal method of fitting pre-measured ZLP registered in the same experimental conditions at given *q*'s, as addressed in "The *q*-EELS experimental setup" in Methods (main text). In supplementary Figs. 4a-b, we now incorporate the normalized ZLPs at $q = 0$ and 0.1 $Å^{-1}$ (insets), which reveal that the ZLP widths only marginally increase at $q = 0.1$ $Å^{-1}$ upon the longer acquisition time required for the weaker plasmon excitations at this *q*. In new supplementary Fig. 4c, we show the detailed ZLP removal by the method of fitting pre-measured ZLP, indicating a minimal overlap of the ZLP tail with the light-electron plasmon and the robustness of the plasmon-peak position to this ZLP removal. In Methods (main text), we have revised the session titles into "The *q*-EELS experimental setup for plasmon excitations" and "The STEM-EELS experiments for core-level excitations" in order to be more explicit on the respective spectral processing.

We further compare the Richardson-Lucy (RL) deconvoluted and original spectra at $q = 0.1$ $Å^{-1}$ along ΓX (new supplementary Fig. 4d; the RL algorithm, HREM Research: K. Ishizuka *et al.*, *Microsc. Microanal*. **9** (Suppl. 2), 832-833 (2003)). The RL deconvolution is renowned for improving the energy resolution and serves as a software monochromator capable of revealing and sharpening weak spectral features [A. Gloter *et al.*, *Ultramicroscopy* **96**, 385-400 (2003); K. Ishizuka *et al.*, *Microsc. Microanal*. **9** (Suppl. 2), 832-833 (2003)]. This numerical method is, meanwhile, well-known for being susceptible for imposing wavy spectral artifacts that carry no electronic significance and would degrade the spectral quality [A. Gloter *et al.*, *Ultramicroscopy* **96**, 385-400 (2003)]. In new supplementary Fig. 4d, the RL deconvolution does improve the energy resolution from ~0.54 eV to ~0.45 eV and sharpen the light-electron plasmon, with the peak position largely remaining intact (inset). Nonetheless, wavy-ripple artifacts are introduced (arrows, new supplementary Fig. 4d) and discount the overall quality. We had been aware of such artificial effects in the RL deconvolution and, therefore, not tended to adopt the method in this work.

Moreover, ZLP represents the fundamental input in the RL deconvolution [A. Gloter *et al.*, *Ultramicroscopy* **96**, 385-400 (2003); K. Ishizuka *et al.*, *Microsc. Microanal*. **9** (Suppl. 2), 832-833 (2003)] and the ZLP removal in the RL-deconvoluted spectra is to be separately conducted (the RL algorithm, HREM Research: K. Ishizuka *et al.*, *Microsc. Microanal*. **9** (Suppl. 2), 832-833 (2003)). The common ZLP-removal method of fitting pre-measured ZLP, however, becomes inapplicable in this regard due to the lack of such an essential reference spectrum. The ZLP removal in the RL spectra thus turns out to be an additional issue on its own and this is the other reason for our decision

on having avoided the RL deconvolution in this work. Otherwise, new supplementary Figs. 4e-f are the ΓY counterparts to new supplementary Figs. 4c-d. Besides, the works by A. Gloter *et al.* and K. Ishizuka *et al.* have been incorporated as new Refs. 3 and 4, respectively, in the supplementary information, with the associated renumbering of all following references.

**REVIEWERS' COMMENTS**

Reviewer #3 (Remarks to the Author):

The authors have shown convincingly that their approach leads to a more reliable background substraction of the spectra. I have no other comments.

## POINT-BY-POINT RESPONSES TO THE REVIEWER'S COMMENTS

The Reviewer's positive comment is encouraging. In this resubmitted package, all changes made in the manuscript in accordance with the editorial requests are in RED for clarity. The associated changes made in supplementary information nonetheless remain BLACK considering the file is not going to be edited by the editorial office and the form in BALCK could warrant its direct publication without further editorial requests for turning all contents into black.

### Reviewer #3 (Remarks to the Author):

**The authors have shown convincingly that their approach leads to a more reliable background subtraction of the spectra. I have no other comments.**

### Response:

We are delighted with the referee's positive remark on our methodology.